PROCEEDINGS A

rspa.royalsocietypublishing.org

Research

Cite this article: Cooray H, Huppert HE, Neufeld JA. 2016 Maximal liquid bridges between horizontal cylinders. *Proc. R. Soc. A* **472**: 20160233.
http://dx.doi.org/10.1098/rspa.2016.0233

Received: 31 March 2016
Accepted: 28 July 2016

Subject Areas:
fluid mechanics, mathematical modelling, applied mathematics

Keywords:
fluid statics, liquid bridges, liquid interfaces, Laplace–Young equation

Author for correspondence:
Himantha Cooray
e-mail: himantha@cantab.net

Maximal liquid bridges between horizontal cylinders

Himantha Cooray[1], Herbert E. Huppert[1,2,3] and Jerome A. Neufeld[1,4,5]

[1]Institute of Theoretical Geophysics, Department of Applied Mathematics and Theoretical Physics, University of Cambridge, Centre for Mathematical Sciences, Wilberforce Road, Cambridge CB3 0WA, UK
[2]Faculty of Science, University of Bristol, Bristol BS8 1UH, UK
[3]School of Mathematics and Statistics, University of New South Wales, Sydney, New South Wales 2052, Australia
[4]BP Institute, Bullard Laboratories and [5]Department of Earth Sciences, Bullard Laboratories, University of Cambridge, Madingley Road, Cambridge CB3 0EZ, UK

HC, 0000-0001-5149-3712

We investigate two-dimensional liquid bridges trapped between pairs of identical horizontal cylinders. The cylinders support forces owing to surface tension and hydrostatic pressure that balance the weight of the liquid. The shape of the liquid bridge is determined by analytically solving the nonlinear Laplace–Young equation. Parameters that maximize the trapping capacity (defined as the cross-sectional area of the liquid bridge) are then determined. The results show that these parameters can be approximated with simple relationships when the radius of the cylinders is small compared with the capillary length. For such small cylinders, liquid bridges with the largest cross-sectional area occur when the centre-to-centre distance between the cylinders is approximately twice the capillary length. The maximum trapping capacity for a pair of cylinders at a given separation is linearly related to the separation when it is small compared with the capillary length. The meniscus slope angle of the largest liquid bridge produced in this regime is also a linear function of the separation. We additionally derive approximate solutions for the profile of a liquid bridge, using the linearized Laplace–Young equation. These solutions analytically verify the above-mentioned relationships obtained for the maximization of the trapping capacity.

THE ROYAL SOCIETY PUBLISHING

1. Introduction

The trapping of a fluid in contact with a solid is a general problem with applications in biological, engineering, industrial and geological processes. Generally, a volume of liquid trapped by two or more solid surfaces and immersed in a different fluid is called a 'liquid bridge'. The trapping is achieved by balancing the weight of the liquid with the surface tension forces acting along the three-phase contact lines and the forces of hydrostatic pressure exerted on the solid–liquid contact surfaces. A detailed review of liquid bridges can be found in Butt & Kappl [1]. Liquid bridges are a very common occurrence in granular matter and porous media. Examples include trapping of water in sand, which acts as an adhesive in sand castles [2], and capillary trapping of supercritical carbon dioxide in porous rocks [3] during carbon dioxide sequestration.

In this paper, we study two-dimensional liquid bridges produced between pairs of horizontal cylinders. A study in this simplified geometry is a first step in the detailed understanding of trapping in porous media. It can also give insights into the behaviour of a three-dimensional liquid bridge trapped between cylindrical rods. Liquid absorption to textiles [4] and retention of water droplets on spider webs are common examples of trapping in this geometry. Additionally, it has recently been proposed as a method of handling and mixing small volumes of liquid in analytical research [5]. Princen [6] and Lukas & Chaloupek [4] solved this problem in two dimensions neglecting the effects of gravity. Such solutions lose their accuracy as the amount of trapped liquid increases. Although three-dimensional profiles of trapped droplets have been studied experimentally [7,8] and numerically [9,10], there is no straightforward method to determine how much liquid a given geometry can trap.

Capillary trapping in other related geometries has been studied using a variety of methods. Urso *et al.* [11] analysed trapping of a liquid in a two-dimensional porous medium comprised of horizontal cylinders. They studied trapping in the limit of small liquid volumes, where gravitational effects can be neglected and the liquid–fluid interfaces may be approximated by circular arcs. Chen *et al.* [12] determined the shape of a three-dimensional liquid bridge trapped between vertical plates using a perturbation method in which the weight of the liquid was neglected, and calculated numerically, using a finite-element method, cases in which the weight was incorporated. Haynes *et al.* [13] solved for the shape of a two-dimensional liquid bridge trapped between a pair of vertical walls using an asymptotic method, in the limit of small liquid weights, and determined the smallest volume of liquid with which a liquid bridge can form. While a two-dimensional liquid bridge is approximately symmetric in the vertical if its weight is close to zero, the shape becomes significantly asymmetric when more liquid is added. The shape of the lower interface in this regime can be modelled as a pendant drop. Profiles of pendant drops have been studied extensively for two-dimensional [14,15] and axially symmetric [16,17] cases. Although the above-mentioned solutions take all the physical parameters into account, they are either analytical solutions that give complicated expressions or numerical solutions and, as a result, do not provide direct expressions to determine the trapping capacity.

The study in this paper starts with an exact solution for the profile of a two-dimensional liquid bridge of arbitrary volume. Results obtained using this solution show very simple approximate relationships governing the maximum trapping capacity: the maximum trapping capacity is linearly related to the separation between the cylinders when the separation is small compared with the capillary length; and the separation that produces the largest trapping capacity is twice the capillary length. We then analytically verify these limiting relationships using several approximate solutions for the shape of a liquid ridge.

2. Theoretical setting

We consider a two-dimensional, horizontally symmetric liquid bridge produced between a pair of identical horizontal cylinders, as shown in figure 1. The weight of the liquid is balanced by the forces of surface tension and the reaction to the hydrostatic pressure exerted by the cylinders. Both liquid–fluid interfaces of the liquid bridge meet the cylinders at a fixed contact angle θ,

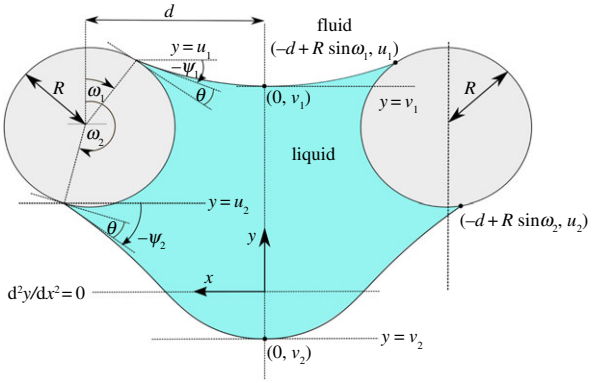

Figure 1. A liquid bridge formed between a pair of horizontal cylinders. θ is the contact angle, ω_1 and ω_2 are the angles from the vertical where the liquid meets the cylinder and ψ_1 and ψ_2 are the interfacial slope angles, which are positive if measured anticlockwise. All the lengths are non-dimensionalized by dividing by the capillary length. The height y is proportional to the pressure of the liquid at the liquid–fluid interface relative to the pressure of the fluid. At $y = 0$, the pressure difference between the two phases and the interfacial curvature are 0. R is the radius of the cylinders and d is the half distance between their centres.

which is in practice locally determined by the fluid and solid surface energies. The interfacial slope angles at the contacts are given by ψ_i, where the subscript $i = 1$ denotes the upper interface and $i = 2$ denotes the lower interface, and ψ_i is positive if the interface slopes upwards leaving the cylinder. The point of contact between a cylinder and an interface is denoted by the angle ω_i to the vertical. The following relationships between ψ_i, θ and ω_i are obtained by consideration of the geometry of the system

$$\psi_1 = \theta - \omega_1 \tag{2.1}$$

and

$$\psi_2 = \pi - \theta - \omega_2. \tag{2.2}$$

The shape of each liquid interface of the liquid bridge is governed by the nonlinear Laplace–Young equation that relates the pressure difference across the interface to its curvature. If the height Y of the interface is given as a function of the horizontal position X by $Y = G(X)$, then the Laplace–Young equation is written as

$$G = \ell_c^2 P(X) \frac{G_{XX}}{[G_X^2 + 1]^{3/2}}, \tag{2.3}$$

where $Y = 0$ is chosen for simplicity in the following calculation as the vertical location where the interfacial curvature (and hence the pressure difference across the interface) is zero. The subscripts in (2.3) denote horizontal derivatives and ℓ_c is the capillary length,

$$\ell_c \equiv \sqrt{\frac{\gamma}{\Delta\rho g}}, \tag{2.4}$$

in which γ is the liquid–fluid interfacial tension, $\Delta\rho$ is the density difference between the liquid and the fluid and g is the acceleration owing to gravity. $P(X) = \pm 1$ depending on whether the liquid phase is below or above the fluid phase, and it is defined as

$$P(X) = \mathrm{sgn}\{D[X, G(X) - \delta] - D[X, G(X) + \delta]\}, \tag{2.5}$$

where $D(X, Y)$ is the density at a location (X, Y) covered by a fluid, which is assumed to be constant within each phase, and δ is a positive infinitesimal length.

Owing to the symmetry of the system, we need to solve only for a half of the bridge to determine its full shape. (In the solution presented here, we consider the left-hand side only). However, writing the Laplace–Young equation in the form of (2.3) has several drawbacks. First, it

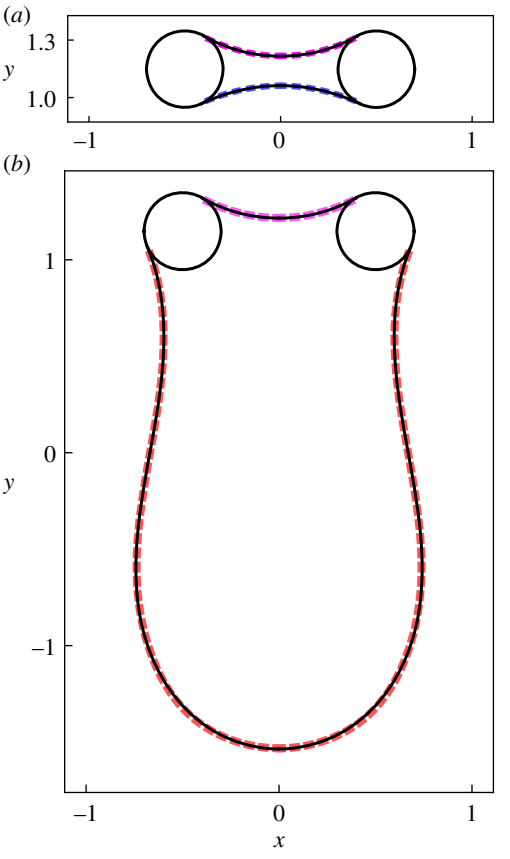

Figure 2. Shapes of two liquid bridges obtained, using exact and approximate solutions of the Laplace–Young equation. Some values of ψ_1 can produce two different liquid bridges, because (2.12) can have two solutions for ψ_2. Both liquid bridges shown here are obtained using the same input parameters $R = 0.2$, $d = 0.5$, $\theta = 0$ and $\psi_1 = -\pi/6$ and represent two solutions for ψ_2, i.e. 0.44 in (*a*) and −1.17 in (*b*). The black solid curves are obtained from the solution to the nonlinear Laplace–Young equation (3.10). The magenta dashed curves show an approximation (4.4) for the shapes of the upper interfaces of the liquid bridges obtained by solving the linearized Laplace–Young equation. The blue dashed curve in (*a*) shows a similar approximation (4.9) for the lower interfaces which is valid when the interfacial slopes are small. The red dashed curve in (*b*) is a composite approximation for the shape of the lower interface, valid for distended liquid bridges, given by (4.30). The results show very good agreement between the exact and approximate solutions.

cannot be solved by direct integration and, second, the shape of the lower interface can be multivalued relative to X and also $P(X)$ can change sign within a single fluid interface (for example, consider the lower fluid interface of the liquid bridge shown in figure 2*b*). These problems can be avoided by instead expressing the interfacial shape as a function of Y. It is also convenient to non-dimensionalize all the lengths with respect to the capillary length and define $x = X/\ell_c$ and $y = Y/\ell_c$. The interfacial shape can then be written as

$$x = f(y), \tag{2.6}$$

where $x = 0$ is the axis of symmetry and $y = 0$ represents the vertical coordinate at which $\mathrm{d}^2 f/\mathrm{d}y^2 = 0$, which is not known *a priori* and has to be determined as a part of the solution. The non-dimensionalized Laplace–Young equation is

$$y = p(y)\frac{f_{yy}}{(f_y^2 + 1)^{3/2}}, \tag{2.7}$$

with $p(y) = \pm 1$ according to the relative positions of the liquid and fluid. Because the interfacial shape is defined as a function of the vertical coordinate, $p(y)$ is now determined by whether the liquid phase is located in the right-hand side or left-hand side of the fluid phase, so that

$$p(y) = \mathrm{sgn}\{D_n[f(y) - \epsilon, y] - D_n[f(y) + \epsilon, y]\} \tag{2.8}$$

as $\epsilon \to 0$, from above, where $D_n(x, y)$ is the fluid density at a location (x, y) which is specified in terms of the non-dimensionalized coordinates. Because only a half of a liquid bridge is to be solved, p is constant within each interfacial segment we consider and it depends only on the direction of the meniscus slope at the contact point

$$p = \begin{cases} \mathrm{sgn}(\psi_1) & \text{for the upper meniscus} \\ -\mathrm{sgn}(\psi_2) & \text{for the lower meniscus.} \end{cases} \tag{2.9}$$

The liquid bridge shown in figure 1 is trapped between cylinders of (non-dimensionalized) radius R and a centre-to-centre distance d. If the vertical coordinates of the contact point and middle point of each interface of the liquid bridge are $y = u_i$ and $y = v_i$, respectively, the interfacial slope angle defines a boundary condition at each contact point

$$f_y(u_i) = -\cot(\psi_i), \tag{2.10}$$

and the requirement for symmetry provides a boundary condition at the centre line

$$\lim_{y \to v_i} f_y = -\mathrm{sgn}(\psi_i)\infty. \tag{2.11}$$

Finally, we impose that the free surfaces intersect the cylinder at the points

$$f(u_i) = d - R\sin\omega_i, \tag{2.12}$$

and are continuous across the centre line

$$f(v_i) = 0. \tag{2.13}$$

In the following section, we obtain a solution for the full shape of the liquid bridge given R, θ, d and ω_1 (or ψ_1) and predict ω_2, u_i and v_i as part of the solution.

3. Exact solution of the nonlinear Laplace–Young equation

The Laplace–Young equation given in (2.7) may be integrated and rearranged to obtain

$$f_y = p' \frac{(1/2)y^2 - a_i}{\sqrt{1 - ((1/2)y^2 - a_i)^2}}, \tag{3.1}$$

where a_i is a constant of the integration and $p' = \pm 1$. To determine the value of p', we differentiate equation (3.1) to obtain

$$f_{yy} = p' \frac{y}{[1 - ((1/2)y^2 - a_i)^2]^{3/2}}. \tag{3.2}$$

Comparison of this result with (2.7) shows that

$$p' = p. \tag{3.3}$$

Substitution of f_y given by (3.1) into (2.11), which denotes the meniscus slope at the mid-point of each interface, yields

$$a_i = \tfrac{1}{2}v_i^2 + q, \tag{3.4}$$

where

$$q = p\,\mathrm{sgn}(\psi_i). \tag{3.5}$$

The value of p in (2.9) is combined with (3.5) to produce

$$q = \begin{cases} 1 & \text{for the upper meniscus} \\ -1 & \text{for the lower meniscus.} \end{cases} \tag{3.6}$$

We then combine (2.10), which gives the meniscus slope at a contact point, with (3.1) and (3.4) to obtain

$$u_i^2 = v_i^2 + 2q(1 - \cos\psi_i). \tag{3.7}$$

The general shape of an interface is determined by integration of (3.1). This integration is carried out using the substitution

$$\tfrac{1}{2}y^2 - a_i = \cos\alpha, \tag{3.8}$$

which transforms (3.1) to

$$f_\alpha = -p\frac{\cos\alpha}{2\sqrt{a_i + \cos\alpha}}. \tag{3.9}$$

The interface may therefore be described completely by the expression

$$f(y) = p\{-\mathrm{sgn}(y)g(y) + [\mathrm{sgn}(y) - \mathrm{sgn}(v_i)]g(0) + \mathrm{sgn}(v_i)g(v_i)\}, \tag{3.10}$$

where the shape in y is given by

$$g(y) = \sqrt{2(1+q) + v_i^2}\,E\left[\frac{1}{2}\cos^{-1}\left(\frac{y^2 - v_i^2}{2} - q\right), \frac{4}{2(1+q) + v_i^2}\right] - \frac{2q + v_i^2}{\sqrt{2(1+q) + v_i^2}}F\left[\frac{1}{2}\cos^{-1}\left(\frac{y^2 - v_i^2}{2} - q\right), \frac{4}{2(1+q) + v_i^2}\right], \tag{3.11}$$

written here in terms of incomplete elliptic integrals $E(\sigma, k)$ and $F(\sigma, k)$ [18]. Equation (3.11) satisfies the boundary condition $f(v_i) = 0$ and remains continuous at $y = 0$.

According to the Laplace–Young equation, the pressure in the liquid side of the interface is higher than the pressure in the fluid side when a liquid surface is convex. As a result, a convex liquid surface corresponds to a negative y and a concave liquid surface corresponds to a positive y. If the lower interface of the liquid bridge slopes downwards at the contact point (i.e. $\psi_2 < 0$), then it has to be convex at the mid-point ($x = 0$) to satisfy the symmetry. This makes v_2 negative. If ψ_2 is positive, then the interface is concave in the middle and v_2 is therefore positive. Using a similar argument also for the upper interface, one can obtain the following general relationship for a liquid bridge,

$$\mathrm{sgn}(v_i) = -q\,\mathrm{sgn}(\psi_i). \tag{3.12}$$

Equation (3.12) can be used to eliminate $\mathrm{sgn}(v_i)$ from (3.10) to obtain

$$f(y) = p\{-\mathrm{sgn}(y)g(y) + [\mathrm{sgn}(y) + q\,\mathrm{sgn}(\psi_i)]g(0) - q\,\mathrm{sgn}(\psi_i)g(v_i)\}, \tag{3.13}$$

and v_i can be eliminated from (3.11) using (3.7) to produce

$$g(y) = \sqrt{2(1 + q\cos\psi_i) + u_i^2}\,E\left[\frac{1}{2}\cos^{-1}\left(\frac{y^2 - u_i^2}{2} - q\cos\psi_i\right), \frac{4}{2(1 + q\cos\psi_i) + u_i^2}\right] - \frac{2q\cos\psi_1 + u_i^2}{\sqrt{2(1 + q\cos\psi_i) + u_i^2}}F\left[\frac{1}{2}\cos^{-1}\left(\frac{y^2 - u_i^2}{2} - q\cos\psi_i\right), \frac{4}{2(1 + q\cos\psi_i) + u_i^2}\right]. \tag{3.14}$$

We now use the boundary condition that defines the horizontal position of the contact point of each menisci given by (2.12) to obtain a relationship between ψ_i and u_i. The geometry of the cylinder gives the relationship between the vertical positions of the upper and lower contact points of the menisci

$$u_2 = u_1 - R(\cos\omega_1 - \cos\omega_2), \tag{3.15}$$

from which ω_i can be replaced using (2.1) and (2.2) to obtain

$$u_2 = u_1 - R[\cos(\theta - \psi_1) + \cos(\theta + \psi_2)]. \tag{3.16}$$

Equations (3.15) and (2.12) with $i = 1, 2$, then represent three equations for ψ_1, ψ_2, u_1 and u_2. If any one of these four parameters is known, the other three can be determined and the shapes of both the menisci can be found.

The following steps show the method used to determine the shapes of the liquid bridges in this paper.

(i) Select the upper point of contact with the cylinder ω_1 and determine ψ_1 using (2.1), or select ψ_1 directly.
(ii) Substitute (3.12), (3.10) and (3.14) into (2.12) and solve for u_1.
(iii) Express u_2 as a function of ψ_2 using (3.16).
(iv) Determine ψ_2 by solving (2.12), into which (3.12), (3.10) and (3.14) are substituted.
(v) Determine ω_2 using (2.2) and
(vi) Obtain the shapes of the menisci using (3.10).

For a given value of ψ_1, (2.12) gives only one solution for u_1. However, for some values of u_2, the solution is multivalued, and thus can give two solutions for ψ_2 resulting in two different liquid bridges as shown in figure 2. The first solution produces a liquid bridge with approximate vertical symmetry and the second solution produces a larger liquid bridge where the lower interface is significantly distended, and as a result, contains a larger amount of liquid compared with the first. Both these solutions are equally valid.

4. Approximate solutions for the shapes of the liquid interfaces

(a) Shape of the upper interface as $|\psi_1| \to 0$

The limit $|\psi_1| \to 0$ corresponds to nearly horizontal upper interfaces. Expressing the shape of the upper meniscus by the function $y = j(x)$ and assuming the interfacial slopes to be small ($j_x \ll 1$), we can write the linearized Laplace–Young equation as

$$j = j_{xx}. \tag{4.1}$$

Solution of this equation with the symmetry boundary condition $j_x(0) = 0$ gives

$$j(x) = c_0 \cosh x, \tag{4.2}$$

where c_0 is a constant to be determined. Because the vertical component of the surface tension force exerted by the cylinders at the contact points is equal to the weight of a liquid meniscus with vertical edges [19,20], the force balance may be written as

$$\int_0^{d - R\sin\omega_1} j\,\mathrm{d}x = -\sin\psi_1. \tag{4.3}$$

This gives the correct value for c_0, and so

$$j(x) = -\sin\psi_1 \frac{\cosh x}{\sinh[d - R\sin(\theta - \psi_1)]} \tag{4.4}$$

which is valid in the region where the meniscus slopes are small. If the absolute value of the meniscus slope angle $|\psi_1|$ is small, then this solution is valid throughout the meniscus, and if $|\psi_1|$

is large, then the solution is valid far (compared with ℓ_c) away from the contact points. As a result, the approximation for v_1 obtained using (4.4) is in general more accurate than the approximation for u_1 obtained using the same equation. The height of the mid-point of the meniscus is therefore obtained using (4.4) and is

$$v_1 = -\sin\psi_1 \operatorname{cosech}[d - R\sin(\theta - \psi_1)], \tag{4.5}$$

and u_1 is to be determined using (3.7), which is a relationship between u_1^2 and v_1^2 derived from the nonlinear Laplace–Young equation. The upper interface cannot pass through $y = 0$, because the interface is convex to the fluid side when $y < 0$ and convex to the liquid side when $y > 0$ according to the Laplace–Young equation. Therefore, we have

$$\operatorname{sgn}(u_1) = \operatorname{sgn}(v_1), \tag{4.6}$$

where $\operatorname{sgn}(v_1)$ is given by (3.12). Using (4.5), (4.6) and (3.6) on (3.7), we obtain

$$u_1 = -\operatorname{sgn}(\psi_1)\sqrt{\sin^2\psi_1 \operatorname{cosech}^2[d - R\sin(\theta - \psi_1)] + 2(1 - \cos\psi_1)} \tag{4.7}$$

for the contact height of the meniscus.

(b) Shape of the lower interface

(i) Solution for small liquid volumes, $|\psi_2| \to 0$

In the limit of small liquid volumes, the upper and lower interfaces are nearly symmetric. If the shape of the lower meniscus is given by $y = k(x)$, then the linearized Laplace–Young equation is

$$k = -k_{xx}. \tag{4.8}$$

This is solved in a manner similar to the upper interface to obtain

$$k(x) = -\sin\psi_2 \frac{\cos x}{\sin[d - R\sin(\theta + \psi_2)]}, \tag{4.9}$$

which gives

$$v_2 = -\sin\psi_2 \csc[d - R\sin(\theta + \psi_2)]. \tag{4.10}$$

For small values of $|\psi_2|$, we have

$$\operatorname{sgn}(u_2) = \operatorname{sgn}(v_2). \tag{4.11}$$

Substitution of equations (4.10) and (4.11) into (3.7) and (3.12) produces

$$u_2 = \operatorname{sgn}(\psi_2)\sqrt{\sin^2\psi_2 \csc^2[d - R\sin(\theta + \psi_2)] - 2(1 - \cos\psi_2)}. \tag{4.12}$$

Equation (4.7) gives the value of u_1 for a given ψ_1. This is substituted into (3.16) to express u_2 as a function of ψ_2,

$$\begin{aligned} u_2 = &-\operatorname{sgn}(\psi_1)\sqrt{\sin^2\psi_1 \operatorname{cosech}^2[d - R\sin(\theta - \psi_1)] + 2(1 - \cos\psi_1)} \\ &- R[\cos(\theta - \psi_1) + \cos(\theta + \psi_2)]. \end{aligned} \tag{4.13}$$

Equations (4.13) and (4.12) together provide an implicit equation for ψ_2. With this result, (4.4) and (4.9) give the shapes of the upper and lower interfaces for any given ψ_1 in the limit of small interfacial slopes. The shape of a liquid bridge determined using this method is shown in figure 2*a* as the magenta and blue dashed curves. It is a very good approximation for the solution obtained using the nonlinear Laplace–Young equation.

(ii) Approximation of the elliptic integrals

The solution to the nonlinear Laplace–Young equation was given as a function of elliptic integrals in (3.10). Here, we introduce an approximation to these integrals for the lower meniscus in order

to obtain simpler relationships that can describe the meniscus shapes and the trapping behaviour. Because $g_2(v_2) = 0$ according to (3.11), the relationship (3.10) reduces, for the lower meniscus, to

$$f_2(y) = -\mathrm{sgn}(y)g(y) + [\mathrm{sgn}(y) - \mathrm{sgn}(v_2)]g(0). \tag{4.14}$$

We now use the values of p and q for the lower meniscus, (2.9) and (3.6), on (3.11) to obtain

$$g_2(y) = |v_2|E\left[\frac{1}{2}\cos^{-1}\left(1 + \frac{y^2 - v_2^2}{2}\right), \left(\frac{2}{v_2}\right)^2\right] - \left(|v_2| - \frac{2}{|v_2|}\right)F\left[\frac{1}{2}\cos^{-1}\left(1 + \frac{y^2 - v_2^2}{2}\right), \left(\frac{2}{v_2}\right)^2\right]. \tag{4.15}$$

The elliptic integrals in equation (4.15) can be replaced using the following transformation formulae [18]

$$F(\sigma, k) = \frac{1}{\sqrt{k}}F\left(\beta, \frac{1}{k}\right) \tag{4.16}$$

and

$$E(\sigma, k) = \sqrt{k}\left[E\left(\beta, \frac{1}{k}\right) - \left(1 - \frac{1}{k}\right)F\left(\beta, \frac{1}{k}\right)\right], \tag{4.17}$$

where

$$\beta = \sin^{-1}(\sqrt{k}\sin\sigma). \tag{4.18}$$

This produces

$$g_2(y) = 2E\left[\sin^{-1}\sqrt{1 - \frac{y^2}{v_2^2}}, \left(\frac{v_2}{2}\right)^2\right] - F\left[\sin^{-1}\sqrt{1 - \frac{y^2}{v_2^2}}, \left(\frac{v_2}{2}\right)^2\right]. \tag{4.19}$$

Substitution of $y = 0$ gives

$$g_2(0) = 2E\left[\left(\frac{v_2}{2}\right)^2\right] - K\left[\left(\frac{v_2}{2}\right)^2\right], \tag{4.20}$$

where $E(k)$ and $K(k)$ are complete elliptic integrals. Byrd & Friedman [18] give series approximations for these functions. Using the first term of each series, we obtain

$$g(y) \approx 2\sqrt{1 - \frac{y^2}{v_2^2}} - \ln\left[\frac{|v_2| - \sqrt{v_2^2 - y^2}}{|y|}\right] \tag{4.21}$$

and

$$g(0) \approx \frac{\pi}{4}\left(2 + \sqrt{4 - v_2^2}\right) - \frac{2\pi}{2 + \sqrt{4 - v_2^2}}. \tag{4.22}$$

Expression (4.22) for $g(0)$ is then used in the next section to determine an approximate solution for the shape of the lower meniscus.

(iii) Solution for large liquid volumes, $|\psi_2| \to \pi/2$

The solution given in §4b(i) is applicable for small $|\psi_2|$ and therefore represents liquid bridges that contain only a small liquid volume. We now introduce a solution for liquid bridges where ψ_2 is close to $\pi/2$, and where the trapped volume is large and hence, to counterbalance the weight of the liquid, the vertical component of the surface tension force is high. In this regime, we focus on the largest liquid bridges, for which $v_2 < 0$ and $u_2 > 0$.

The shape of the upper part of the lower meniscus, near the contact points, may most readily be described by $x = h(y)$ with $h_y \ll 1$. The linearized Laplace–Young equation for this regime is therefore

$$y = h_{yy}, \tag{4.23}$$

which we may solve to obtain

$$x = h(y) = \tfrac{1}{6}y^3 + c_1 y + c_2, \tag{4.24}$$

where c_1 and c_2 are constants. These constants can now be constrained by our solutions to the nonlinear Laplace–Young equation. We first recall the constrains (3.4) and (3.1), obtained in the solution of the nonlinear Laplace–Young equation, which gives

$$f_y(0) = \frac{1 - (1/2)v_2^2}{|v_2|\sqrt{1 - (1/4)v^2}}. \tag{4.25}$$

We use the conditions $h_y(0) = f_y(0)$ and $h(0) = f(0)$, where $f(0)$ is given by the approximation (4.22), to determine c_1 and c_2. Thus, we have

$$h(y) = \frac{1}{6}y^3 + \frac{1 - (1/2)v_2^2}{|v_2|\sqrt{1 - (1/4)v_2^2}}y + \frac{\pi}{4}\left(2 + \sqrt{4 - v_2^2}\right) - \frac{2\pi}{2 + \sqrt{4 - v_2^2}}, \tag{4.26}$$

which we may combine with the approximation for the upper meniscus determined for $|\psi_1| \to 0$ in §4a. This approximation along with (3.16) produces an expression for u_2, (4.13). Combination of this expression with (3.7) gives

$$\begin{aligned} v_2^2 = \{&\mathrm{sgn}(\psi_1)\sqrt{\sin^2\psi_1 \mathrm{cosech}^2[d - R\ \sin(\theta - \psi_1)] + 2(1 - \cos\psi_1)} \\ &- R[\cos(\theta - \psi_1) + \cos(\theta + \psi_2)]\}^2 + 2(1 - \cos\psi_2). \end{aligned} \tag{4.27}$$

We then use the boundary condition given in (2.12), that the fluid intersects the cylinder

$$h(u_2) = d - R\sin(\theta + \psi_2), \tag{4.28}$$

along with u_2 given by (4.13) and v_2 given by (4.27), to get an equation that may be solved to determine ψ_2. We note that $h(y)$ is a good approximation for the upper part of the lower meniscus, as demonstrated in figure 3.

Once ψ_2, and hence v_2, are determined, the shape of the lower part of the lower meniscus can be obtained approximately. The meniscus slopes in this regime are small relative to the x-axis, and therefore, the linearized Laplace–Young equation, (4.8), is applicable. Solution with the boundary condition $k(0) = v_2$ gives $y = v_2\cos x$, or

$$x = \cos^{-1}\left(\frac{y}{v_2}\right). \tag{4.29}$$

We combine the solutions for the upper part of the lower meniscus (4.26) and lower part of the lower meniscus (4.29) to produce the following empirical expression for the meniscus shape

$$x = \tanh\left[\frac{7}{4}(y - v_2)\right]h(y) + \{1 - \tanh[2(y - v_2)]\}\cos^{-1}\left(\frac{y}{v_2}\right), \tag{4.30}$$

which is valid for the entirety of the lower meniscus as shown in figures 2 and 3.

5. The maximal trapping capacity

A quantity of significant interest in a variety of physical settings is the volume of fluid that may be trapped as a function of the imposed geometry and material properties through the apparent contact angle. Here, we calculate the trapping capacity, which in our two-dimensional geometry is equivalent to the cross-sectional area. We then determine the maximum achievable trapping capacity at a given separation between the cylinders and the separation at which the largest liquid bridge can be produced.

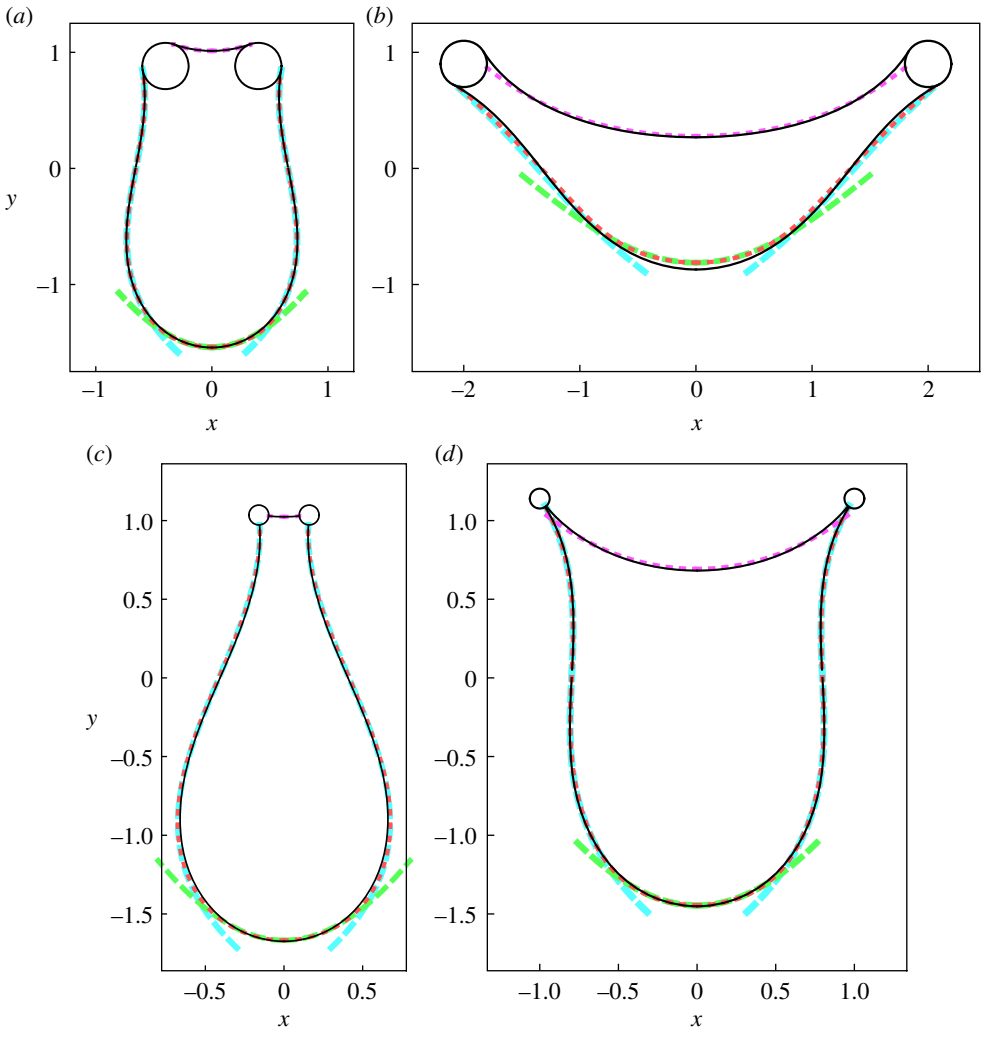

Figure 3. Panels (*a*) and (*b*) show two liquid bridges carrying the same amount of liquid ($A = 3.0$) between a pair of horizontal cylinders with $R = 0.2$ and $\theta = 0$ located at two different separations. The separation d in (*a*) is 0.4, which gives $\psi_1 = -\pi/9$ and $\psi_2 = -1.40$. Parameters in (*b*) are $d = 2.0$, $\psi_1 = -1.01$ and $\psi_2 = -0.48$. Panels (*c*) and (*d*) show shapes of liquid bridges corresponding to the maximum trapping capacities for a pair of cylinders with $R = 0.063$ and $\theta = \pi/2$ at two different separations. The parameters are $d = 0.16$, $A_{\max} = 2.31$, $\psi_{1,A_{\max}} = -0.10$ and $\psi_2 = -1.50$ in (*c*) and $d = 1.0$, $A_{\max} = 3.24$, $\psi_{1,A_{\max}} = -0.88$ and $\psi_2 = -1.00$ in (*d*). The figures show results obtained using both exact and approximate solutions to the Laplace–Young equation. The black solid curves are the solutions to the nonlinear Laplace–Young equation given by (3.13). The magenta dashed curve is the approximation for the shape of the upper interface (4.4) obtained by solving the linearized Laplace–Young equation. The cyan dashed curve and the green dashed curve are the approximations for the shapes of the upper part and the lower part of the lower interface given by (4.26) and (4.29), respectively. The red dashed curve is the composite approximation for the shape of the lower interface (4.30) obtained by combining (4.26) and (4.29). There is excellent agreement between the approximate and exact solutions when $\psi_1 \to 0$ and $|\psi_2| \to \pi/2$. The composite approximation (4.30) covers both (4.26) and (4.29) very well.

(a) The maximum trapping capacity at a given separation

The solution of the nonlinear Laplace–Young equation automatically satisfies a local force balance along the liquid bridge. A simple way to determine the bridge cross-sectional area A is therefore

through a vertical force balance considering the liquid weight and the forces of surface tension and hydrostatic pressure.

$$A = -2(\sin\psi_1 + \sin\psi_2) - R\int_{\omega_1}^{\omega_2} \cos\omega(u_1 - R\cos\omega_1 + R\cos\omega)\,\mathrm{d}\omega. \tag{5.1}$$

Integration and the use of (2.1) and (2.2) to replace ω_i with ψ_i produces

$$A = -2(\sin\psi_1 + \sin\psi_2) + 2Ru_1[\sin(\theta - \psi_1) - \sin(\theta + \psi_2)] + R^2\left[\psi_2 - \psi_1 + 2\theta - \pi + 2\cos(\theta - \psi_1)\sin(\theta + \psi_2) - \frac{\sin 2(\theta - \psi_1) - \sin 2(\theta + \psi_2)}{2}\right]. \tag{5.2}$$

The quantities ψ_2 and u_1 in equation (5.2) can be determined as functions of ψ_1 using the solution of the nonlinear Laplace–Young equation described in §3. By numerical maximization of A with respect to ψ_1, the maximum trapping capacity ($A_{\max}$) and ψ_1 that produces this trapping capacity ($\psi_{1,A_{\max}}$) can be determined for a given combination of R, θ and d. Two representative liquid bridges, corresponding to $A_{\max}$ for different values of d, are shown in figure 3*c*,*d*. This solution process was repeated for a range of R, θ and d, and the behaviour of $A_{\max}$ and $\psi_{1,A_{\max}}$ were analysed. The results are shown by symbols in figure 4*a*,*b*.

Figure 4*a* shows that the maximal trapping capacity, $A_{\max}$ is linearly proportional to the separation, d, when $R \ll 1$ and $d \ll 1$. This relationship can be explained using the approximate solution derived in §4. We define $2s_i$ as the distance between the contact points of a meniscus, that is,

$$s_i = d - R\sin\omega_i, \tag{5.3}$$

so that when $d, R \ll 1$, $s_i \ll 1$ for all ω_i. In this regime, the shape of the upper meniscus has a nearly constant radius of curvature $-s/\sin\psi_1$. As a result, we have

$$|u_1 - v_1| \le s_1. \tag{5.4}$$

Because $s_1 \ll 1$, the amount of liquid trapped above the $y = v_1$ is negligible and because $R \ll 1$, almost all the liquid is trapped as a droplet hanging below $y = u_2$. The cross-sectional area of the part of the liquid bridge below $y = u_2$ is determined by balancing the non-dimensionalized weight of the liquid A with the force of surface tension given by $-2\sin\psi_2$ and the force of hydrostatic pressure given by $2u_2s_2$,

$$A = 2(-\sin\psi_2 + u_2s_2). \tag{5.5}$$

The surface tension force acting on the liquid bridge is more significant compared with the force of hydrostatic pressure, because $s_2 \ll 1$. A is therefore maximized when

$$\psi_2 \approx -\frac{\pi}{2}, \tag{5.6}$$

which is the meniscus slope angle that maximizes the vertical component of the force of surface tension. Using (5.6) and $d - R\sin(\theta + \psi_2) = s_2$ on (4.28) and replacing q_2 and v_2 using (3.6) and (3.7), respectively, we obtain an equation for u_2

$$\left(\frac{1}{6} - \frac{1}{\sqrt{4 - u_2^4}}\right)u_2^3 + \frac{\pi}{4}\left(2 + \sqrt{2 - u_2^2}\right) - \frac{2\pi}{2 + \sqrt{2 - u_2^2}} = s_2. \tag{5.7}$$

As $s \to 0$,

$$u_2 \approx 1 \tag{5.8}$$

is an approximate solution for (5.7). Substitution of (5.6) into (2.2) gives $\sin\omega_2 = -\cos\theta$, which in combination with (5.3) produces

$$s_2 = d + R\cos\theta. \tag{5.9}$$

Substitution of (5.6), (5.9) and (5.8) into (5.5) produces

$$A_{\max} \approx 2(1 + d + R\cos\theta). \tag{5.10}$$

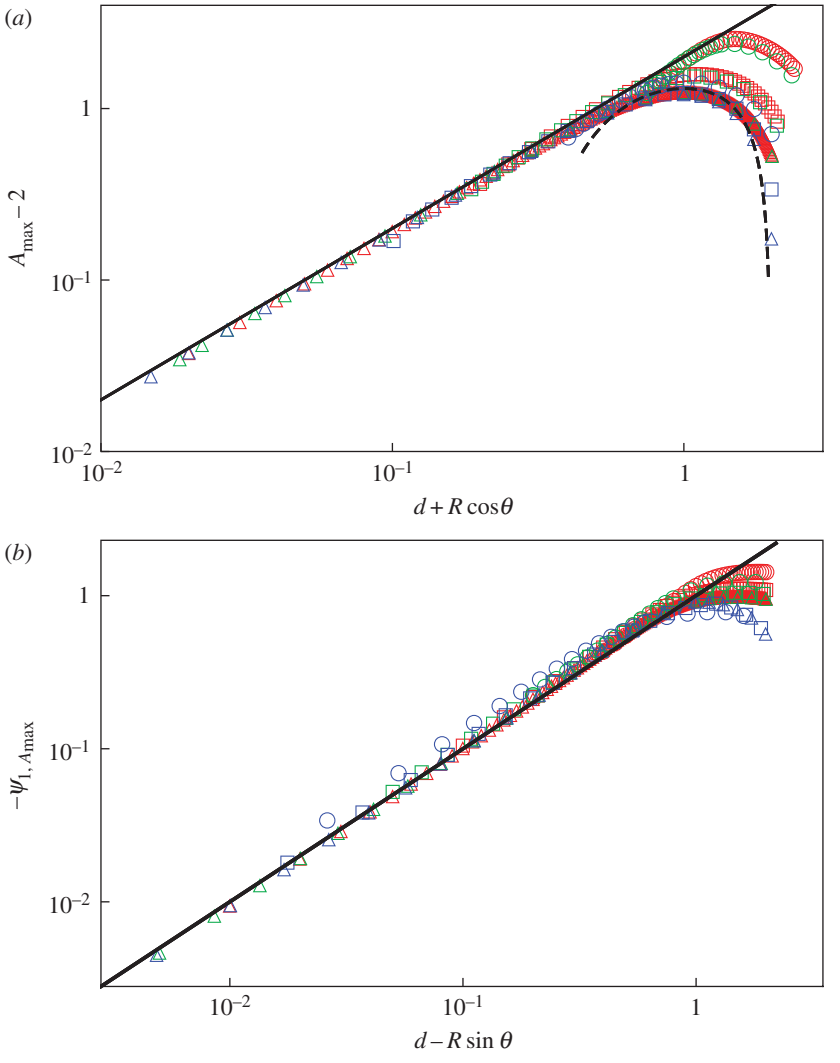

Figure 4. (*a*) The maximum trapping capacity (the cross-sectional area of the largest liquid bridge, A_{max}) between pairs of horizontal cylinders. (*b*) The value of ψ_1 for the largest liquid bridges. Symbols show results obtained for different values of R, θ and d by numerically maximizing A (5.2), determined using the solution of the nonlinear Laplace–Young equation, with respect to ψ_1. Each marker represents a cylinder radius. Triangles denote $R = 0.01$, squares denote $R = 0.1$ and circles denote $R = 0.4$. Colours represent different contact angles. Red symbols (triangle, square, circle) represent $\theta = 0$, green symbols (triangle, square, circle) represent $\theta = \pi/6$ and blue symbols (triangle, square, circle) represent $\theta = \pi/2$. The black curves are approximations for the maximal trapping parameters. In (*a*), the black solid line denotes (5.10), which is valid for small d, and the black dashed curve denotes (5.28), which is valid when d is close to 1. The black solid line in (*b*) is the equation (5.16). The approximate solutions describe the maximal trapping behaviour very well for small R ($R \ll 1$). Both A_{max} and $\omega_{1,A_{max}}$ are linearly related to d when $d \ll 1$.

This is plotted by the black line shown in figure 4*a*. It is a good approximation for small cylinders at close range.

We also observe a linear relationship between d and $\psi_{1,A_{max}}$ for small R and d in figure 4*b*. This relationship can also be verified using the approximate solutions to the Laplace–Young equation. If $|\psi_1|$ is small, (4.4) is valid throughout the upper meniscus, which gives

$$u_1 = -\sin\psi_1 \coth(d - R\sin\omega_1). \tag{5.11}$$

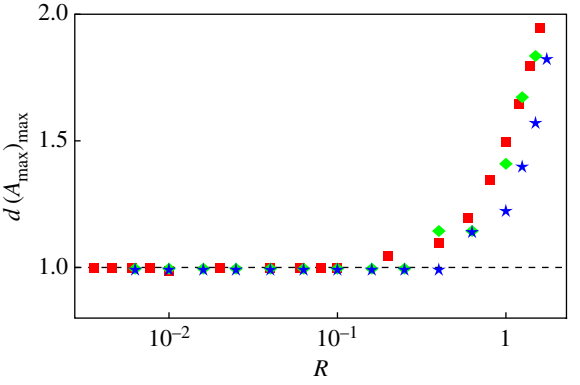

Figure 5. For small cylinders, the maximum trapping capacity $A_{\max}$ maximizes at $d \approx 1$. Figure shows the value of d at which the maximum trapping capacity occurs, obtained using the nonlinear Laplace–Young equation. Red squares are for $\theta = 0$, green diamonds are for $\theta = \pi/6$ and blue stars are for $\theta = \pi/2$.

Because $R \ll 1$, we have

$$u_1 \approx u_2, \tag{5.12}$$

which gives $u_1 \approx 1$ owing to (5.8). Using this result on (5.11), we obtain

$$-\sin\psi_{1,A_{\max}} = \tanh(d - R\sin\omega_{1,A_{\max}}). \tag{5.13}$$

Because $d - R\sin\omega_{1,A_{\max}} = s_1 \ll 1$, equation (5.13) gives

$$-\psi_{1,A_{\max}} \approx d - R\sin\omega_{1,A_{\max}}, \tag{5.14}$$

where ψ_1 and ω_1 are related by (2.1), which gives

$$\omega_1 \approx \theta \tag{5.15}$$

for small ψ_1. Substitution of (5.15) to (5.14) gives the relationship

$$-\psi_{1,A_{\max}} \approx d - R\sin\theta, \tag{5.16}$$

which is plotted by the black line in figure 4*b*. This result approximates the exact solution very well when the cylinder radius and inter-cylinder radius are small compared with the capillary length.

(b) The separation that maximizes the trapping capacity

Figure 4*a* shows that the maximum trapping capacity $A_{\max}$ as a function of d is increasing when $d \ll 1$ and decreasing for large d. Figure 5 plots the value of d in which $A_{\max}$ reaches a maximum ($d(A_{\max})_{\max}$) as a function of R for different values of θ. Interestingly, it shows that $d(A_{\max})_{\max} = 1$ when $R \ll 1$ for all θ. In this section, we analytically explain this result based on the approximate solutions obtained earlier for the liquid bridge geometry.

We assume that (4.4) gives a sufficiently good approximation for u_1

$$u_1 = -\sin\psi_1 \coth s, \tag{5.17}$$

where $s = s_i \approx d$ which is valid when $R \to 0$ according to (5.3). For small R, we also have $u_2 \approx u_1$ which gives

$$u_2 \approx -\sin\psi_1 \coth s, \tag{5.18}$$

and (3.7) then gives

$$v_2^2 \approx \coth^2 s \sin^2\psi_1 - 2\cos\psi_2 + 2. \tag{5.19}$$

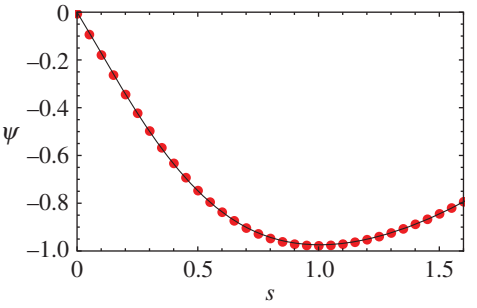

Figure 6. The expression for ψ given in (5.25) (solid curve) is compared with ψ obtained using a numerical solution of (5.20) (red symbols). The figure shows that the analytical expression is an accurate solution for (5.20).

Substitution of the expressions (5.18) and (5.19) obtained for u_2 and v_2 into (4.28) yields

$$m(\psi_1, \psi_2, s) = 0, \tag{5.20}$$

where

$$\begin{aligned} m(\psi_1, \psi_2, s) = &-\frac{1}{6}\coth^3 s \sin^3 \psi_1 \\ &- \frac{\coth s \sin\psi_1 (2\cos\psi_2 - \coth^2 s \ \sin^2\psi_1)}{\sqrt{4 - (\coth^2 s \sin^2\psi_1 - 2\cos\psi_2)^2}} \\ &+ \frac{1}{4}\pi\left(2 + \sqrt{2\cos\psi_2 - \coth^2 s \sin^2\psi_1 + 2}\right) \\ &- \frac{2\pi}{2 + \sqrt{2\cos\psi_2 - \coth^2 s \sin^2\psi_1 + 2}} \\ &- s. \end{aligned} \tag{5.21}$$

Because the contact points of the upper and lower menisci are very close to each other ($u_1 \approx u_2$), we need $\psi_1 \geq \psi_2$ to avoid the two menisci intersecting each other. We now consider the limit $\psi_1 = \psi_2 = \psi$, where (5.20) is written as

$$m(\psi, s) = 0. \tag{5.22}$$

To solve for ψ, $m(\psi, s)$ is expanded in a first-order power series

$$m(\psi, s) = m(\psi_0, s) + (\psi - \psi_0) m_\psi(\psi_0, s). \tag{5.23}$$

A numerical solution of (5.22) shows that $\psi \approx -\frac{7}{4}s$ as $s \to 0$ and $\psi \approx -1$ as $s \to 1$. We therefore select ψ_0 in (5.23) as

$$\begin{aligned} \psi_0(s) &= -\frac{7}{4}s(1-s) - s^2 \\ &= \frac{1}{4}(3s^2 - 7s), \end{aligned} \tag{5.24}$$

which gives the solution

$$\psi(s) = \frac{1}{4}(3s^2 - 7s) - \frac{m[(1/4)(3s^2 - 7s), s]}{m_\psi[(1/4)(3s^2 - 7s), s]}. \tag{5.25}$$

To test the accuracy of the solution for ψ given by (5.25), it is compared with the numerical solution of (5.22). As shown in figure 6, the accuracy of the analytical approximation is very good for a wide range of s.

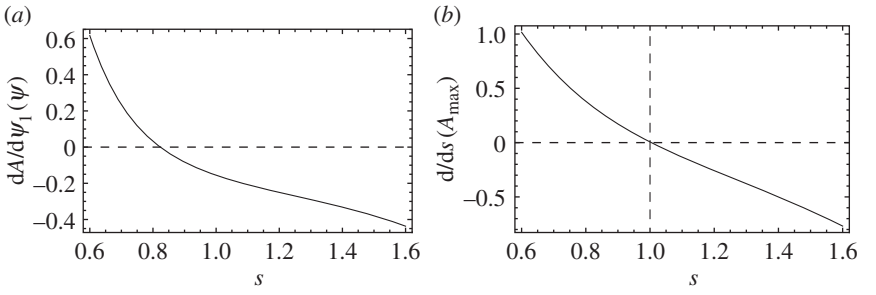

Figure 7. Panel (*a*) shows $\mathrm{d}A/\mathrm{d}\psi_1$ calculated using (5.27) at $\psi_1 = \psi_2 = \psi$. The derivative is negative around $s = 1$ and beyond. Because $u_1 \approx u_2$ and the two menisci should not intersect, the minimum possible value of ψ_1 is ψ. The negative derivative means that A maximizes when $\psi_1 = \psi_2 = \psi$. Panel (*b*) shows the derivative of $\mathrm{d}V/\mathrm{d}s$ calculated at $\psi_1 = \psi_2 = \psi$. A maximizes at $s = 1$.

The force of hydrostatic pressure exerted by small cylinders on a liquid bridge is negligible compared with the force of surface tension, because the solid–liquid contact area is small. The cross-sectional area of the liquid bridge can therefore be calculated by balancing the surface tension force with the weight

$$A = -2(\sin\psi_1 + \sin\psi_2). \tag{5.26}$$

When $\psi_1 = \psi_2 = \psi$ for a given s, we have

$$\frac{\mathrm{d}A}{\mathrm{d}\psi_1}[\psi(s)] = -2\cos\psi\left(1 + \frac{\partial\psi_2}{\partial\psi_1}[\psi(s), s]\right), \tag{5.27}$$

where $\partial\psi_2/\partial\psi_1$ is obtained as a function of ψ_1, ψ_2 and s by differentiating (5.20) with respect to ψ_1.

Figure 7*a* shows that $\partial\psi_2/\partial\psi_1[\psi(s)]$ is negative around $s = 1$, which means the trapping capacity for a given separation of around 1 is maximized when $\psi_1 = \psi_2 = \psi(s)$. The maximum trapping capacity is therefore given by

$$A_{\max} = -4\sin\psi(s). \tag{5.28}$$

For small cylinders, (5.28) gives the value of $A_{\max}$ at far range, whereas (5.10) explains the behaviour at short range as shown in figure 4*a*.

Differentiation of (5.28) gives

$$\frac{\mathrm{d}A_{\max}}{\mathrm{d}s} = -4\cos\psi\frac{\mathrm{d}\psi}{\mathrm{d}s}, \tag{5.29}$$

whereas ψ and $\mathrm{d}\psi/\mathrm{d}s$ can be obtained from (5.25). According to figure 7*b*, $A_{\max}$ is a maximum when $s = 1$. According to the results in figure 5, which are obtained by solving the nonlinear Laplace–Young equation, $A_{\max}$ maximizes at $d \approx 1$ when $R \ll 1$. Both these results are similar, because $d \approx s$ for small R.

6. Conclusion

We present exact solutions to the nonlinear Laplace–Young equation to determine the equilibrium shape of a liquid bridge trapped between a pair of infinitely long horizontal cylinders. We also introduce several simpler solutions that approximate the exact solutions very well.

Both the exact and approximate solutions show that the maximum amount of liquid that can be trapped in a given system and the conditions of this maximization can be approximated by a few simple relationships when the cylinder radius is small compared with the capillary length (ℓ_c). Regardless of the contact angle, the largest liquid bridges form when the inter-cylinder distance is approximately $2\ell_c$. If the inter-cylinder distance is small compared with ℓ_c, the maximum

amount of liquid held by a pair of cylinders is given by the equation $a_{\max} \approx 2\ell_c\,(1 + D + r\cos\theta)$, in which a is the cross-sectional area of the liquid bridge, $2D$ is the inter-cylinder distance, r is the cylinder radius and θ is the contact angle. At this maximum trapping, the meniscus slope angle of the upper interface of the liquid bridge can be approximated by the linear relationship $\psi_{1,a_{\max}} \approx (r\sin\theta - D)/\ell_c$.

The solutions we present here can be extended to determine the equilibrium of fluid ganglia or stringers trapped in a solid matrix, enclosed by a different non-mixing fluid. Although such systems have been studied neglecting gravitational effects [21], an analysis considering the weight of the fluid can help determine the residual trapping capacity of a porous medium. It can also be used to characterize deformations of the solid support induced by the surface tension forces from fluid ganglia and any fluid movement that result from this. This is a significant factor in trapping by a flexible solid support, as shown by Duprat *et al.* [8] for the case of small liquid bridges between cylinders.

The stability of a trapped liquid is another interesting parameter in capillary trapping. This has been investigated, in the absence of gravity, for the trapping between pairs of vertical plates [22, 23], spheres [24] and solid objects with other geometries [25]. The work by Slobozhanin *et al.* [26] on the stability of a liquid trapped inside a solid cylinder is an example of an analysis taking gravity into account. The stability analysis was not a focus of this paper and a comprehensive account of this subject can be found in reference [27].

Ethics. This paper does not include any study that has made use of human or animal subjects or research that requires approval by ethics committees.

Data accessibility. This paper does not include any experimental data. All the results are reproducible using the analytical methods described in the paper.

Authors' contributions. H.C. developed the exact solution of the nonlinear Laplace–Young equation to determine the liquid bridge shapes and drafted the manuscript. H.C., H.E.H. and J.A.N. contributed jointly to the development of the approximate solutions for the shapes of the liquid interfaces, analysis of the results and to the development of the manuscript.

Competing interests. We have no competing interests.

Funding. This work is supported under the EU TRUST consortium. H.E.H. was partially supported by a Leverhulme Emeritus Professorship during this research. J.A.N. is partially supported by a Royal Society University Research Fellowship.

Acknowledgements. We thank Raphael Blumenfeld for many useful discussions.

References

1. Butt H-J, Kappl M. 2009 Normal capillary forces. *Adv. Colloid Interface Sci.* **146**, 48–60. (doi:10.1016/j.cis.2008.10.002)
2. Schiffer P. 2005 Granular physics: a bridge to sandpile stability. *Nat. Phys.* **1**, 21–22. (doi:10.1038/nphys129)
3. Juanes R, MacMinn CW, Szulczewski ML. 2009 The footprint of the CO_2 plume during carbon dioxide storage in saline aquifers: storage efficiency for capillary trapping at the basin scale. *Transp. Porous Media* **82**, 19–30. (doi:10.1007/s11242-009-9420-3)
4. Lukas D, Chaloupek J. 2003 Wetting between parallel fibres; column-unduloid and column disintegration transitions. *Proc. Inst. Mech. Eng. Part H, J. Eng. Med.* **217**, 273–277. (doi:10.1243/095441103322060721)
5. Cheong BH-P, Lye JKK, Backhous S, Liew OW, Ng TW. 2013 Microplates based on liquid bridges between glass rods. *J. Colloid Interface Sci.* **397**, 177–184. (doi:10.1016/j.jcis.2013.01.043)
6. Princen H. 1970 Capillary phenomena in assemblies of parallel cylinders: III. Liquid columns between horizontal parallel cylinders. *J. Colloid Interface Sci.* **34**, 171–184. (doi:10.1016/0021-9797(70)90167-0)
7. Protiere S, Duprat C, Stone HA. 2013 Wetting on two parallel fibers: drop to column transitions. *Soft Matter* **9**, 271–276. (doi:10.1039/c2sm27075g)
8. Duprat C, Protière S, Beebe AY, Stone HA. 2012 Wetting of flexible fibre arrays. *Nature* **482**, 510–513. (doi:10.1038/nature10779)
9. Wu X-F, Bedarkar A, Vaynberg KA. 2010 Droplets wetting on filament rails: surface energy and morphology transition. *J. Colloid Interface Sci.* **341**, 326–332. (doi:10.1016/j.jcis.2009.09.019)

10. Bedarkar A, Wu X-F, Vaynberg A. 2010 Wetting of liquid droplets on two parallel filaments. *Appl. Surf. Sci.* **256**, 7260–7264. (doi:10.1016/j.apsusc.2010.05.061)
11. Urso M, Lawrence C, Adams M. 1999 Pendular, funicular, and capillary bridges: results for two dimensions. *J. Colloid Interface Sci.* **220**, 42–56. (doi:10.1006/jcis.1999.6512)
12. Chen T-Y, Tsamopoulos JA, Good RJ. 1992 Capillary bridges between parallel and non-parallel surfaces and their stability. *J. Colloid Interface Sci.* **151**, 49–69. (doi:10.1016/0021-9797(92)90237-G)
13. Haynes M, O'Brien SBG, Benilov ES. 2016 Asymptotics of a horizontal liquid bridge. *Phys. Fluids* **28**, 042107. (doi:10.1063/1.4946001)
14. Pitts E. 1973 The stability of pendent liquid drops. Part 1. Drops formed in a narrow gap. *J. Fluid Mech.* **59**, 753–767. (doi:10.1017/S0022112073001849)
15. Majumdar SR, Michael DH. 1976 The equilibrium and stability of two dimensional pendent drops. *Proc. R. Soc. Lond. A* **351**, 89–115. (doi:10.1098/rspa.1976.0131)
16. Orr FM, Scriven LE, Rivas AP. 1975 Pendular rings between solids: meniscus properties and capillary force. *J. Fluid Mech.* **67**, 723–742. (doi:10.1017/S0022112075000572)
17. Boucher EA, Evans MJB. 1975 Pendent drop profiles and related capillary phenomena. *Proc. R. Soc. Lond. A* **346**, 349–374. (doi:10.1098/rspa.1975.0180)
18. Byrd PF, Friedman MD. 1971 *Handbook of elliptic integrals for engineers and scientists*. Berlin, Germany: Springer.
19. Vella D, Mahadevan L. 2005 The 'Cheerios effect'. *Am. J. Phys.* **73**, 817. (doi:10.1119/1.1898523)
20. Keller JB. 1998 Surface tension force on a partly submerged body. *Phys. Fluids* **10**, 3009. (doi:10.1063/1.869820)
21. Niven RK. 2006 Force stability of pore-scale fluid bridges and ganglia in axisymmetric and non-axisymmetric configurations. *J. Pet. Sci. Eng.* **52**, 1–18. (doi:10.1016/j.petrol.2006.03.015)
22. Vogel TI. 1987 Stability of a liquid drop trapped between two parallel planes. *SIAM J. Appl. Math.* **47**, 516–525. (doi:10.1137/0147034)
23. Vogel TI. 1989 Stability of a liquid drop trapped between two parallel planes II: general contact angles. *SIAM J. Appl. Math.* **49**, 1009–1028. (doi:10.1137/0149061)
24. Vogel TI. 2013 Liquid bridges between balls: the small volume instability. *J. Math. Fluid Mech.* **15**, 397–413. (doi:10.1007/s00021-012-0117-y)
25. Fel LG, Rubinstein BY. 2015 Stability of axisymmetric liquid bridges. *Z. Angew. Math. Phys.* **66**, 3447–3471. (doi:10.1007/s00033-015-0555-5)
26. Slobozhanin LA, Alexander JID, Fedoseyev AI. 1999 Shape and stability of doubly connected axisymmetric free surfaces in a cylindrical container. *Phys. Fluids* **11**, 3668–3677. (doi:10.1063/1.870230)
27. Langbein DW. 2002 *Capillary surfaces: shape–stability–dynamics, in particular under weightlessness*, vol. 178. Berlin, Germany: Springer Science & Business Media.